LA-UR-11-10640
Approved for public release; distribution is unlimited.

Title: Imaging Faults with Reverse-Time Migration for Geothermal Exploration at Jemez Pueblo in New Mexico

Author(s): Huang, Lianjie
Albrecht, Michael
Kaufman, Greg
Kelley, Shari
Rehfeldt, Kenneth
Zhang, Zhifu

Intended for: GRC's 35th Annual Meeting, 2011-10-23/2011-10-26 (San Diego, California, United States)

Imaging Faults with Reverse-Time Migration for Geothermal Exploration at Jemez Pueblo in New Mexico

Lianjie Huang
Los Alamos National Laboratory, Geophysics Group, MS D443, Los Alamos, NM 87545

Shari Kelley
New Mexico Bureau of Geology and Mineral Resources, New Mexico Tech, Socorro, NM 87801

Zhifu Zhang and Kenneth Rehfeldt
Los Alamos National Laboratory, Geophysics Group, MS D443, Los Alamos, NM 87545

Michael Albrecht
TBA Power, 2825 East Cottonwood Parkway, Suite 500, Salt Lake City, Utah 84121

Greg Kaufman
Department of Resource Protection, PC Box 100, Jemez Pueblo, NM 87024

Abstract

The fault zones at Jemez Pueblo may dominate the flow paths of hot water, or confine the boundaries of the geothermal reservoir. Therefore, it is crucial to image the geometry of these fault zones for geothermal exploration in the area. We use reverse-time migration with a separation imaging condition to image the faults at Jemez Pueblo. A finite-difference full-wave equation method with a perfectly-matching-layer absorbing boundary condition is used for backward propagation of seismic reflection data from receivers and forward propagation of wavefields from sources. In the imaging region, the wavefields are separated into the upgoing and downgoing waves, and leftgoing and rightgoing waves. The upgoing and downgoing waves are used to obtain the downward-looking image, and the leftgoing and rightgoing waves are used to form the left-looking image and right-looking image from sources. The left-looking and right-looking images are normally weaker than the downward-looking image because the reflections from the fault zones are much weaker than those from sedimentary layers, but these migration results contain the images of the faults. We apply our reverse-time migration with a wavefield separation imaging condition to seismic data acquired at Jemez Pueblo, and our preliminary results reveal many faults in the area.

Introduction

Most previous research on the geothermal system in the Valles caldera area focused on the southwestern margin of the caldera (Fig. 1), including the Sulfur Springs area, Fenton Hill, Soda Dam, San Diego Canyon, and Jemez Springs (Goff et al. 1981; Goff and Grigsby 1982; Goff et al. 1988). Fenton Hill was the test site for the Hot Dry Rock Project in the late 1970s and

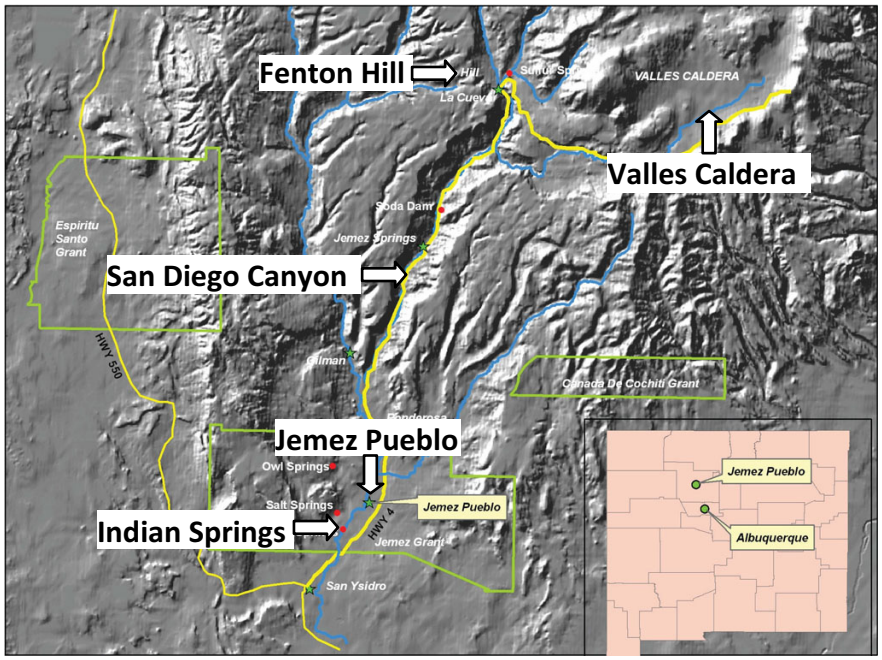

Figure 1: A map showing locations of Valles caldera, Fenton Hill, and the Pueblo of Jemez.

early 1990s (Kerr 1987; Brown 1993). Jemez Springs is the site of commercial hot springs with temperatures up to 72°C. The Pueblo of Jemez is located on the southwestern margin of the Jemez Mountains in north-central New Mexico, USA. Jemez Pueblo is located at approximately 22 miles southwest of the Valles caldera. There are many hot springs on the west and southwest edge of the Valles caldera and down San Diego Canyon.

On the Jemez Pueblo, a hot water spring discharges to the Jemez River. A 240-foot deep well was drilled in 1991 at the Indian Springs. It produced water of 136 F and a flow of 150 gallons per minute (Witcher et al. 1992; Witcher 2004). The purpose of this project is to characterize the geothermal resource at the Jemez Pueblo, which, based on the current work, is anticipated to be located deeper than 3000 feet and located east of the current spring discharge location.

To explore the geothermal resource at Jemez Pueblo, seismic surveys were conducted in December, 2010 along three lines for the purpose of obtain high-resolution subsurface images near the Indian Springs fault zone. This is the first exploration of the deep geothermal reservoir at the Pueblo of Jemez using active-seismic reflection surveys.

Seismic migration is the primary tool for imaging subsurface structures for oil/gas exploration (Claerbout 1985; Fehler and Huang 2002). Wave-equation migration imaging is based on one-way wave propagation to obtain downward-looking images (Stoffa et al. 1990; Huang et al. 1999b, a; Huang and Fehler 2000b, a; Sun et al. 2005). Reverse-time migration uses the full-wave equation to forward and backward propagate the source and receiver wavefields (Chang and McMechan 1986, 1987, 1990; Zhu and Lines 1997; Sun and McMechan 2001; Symes 2007; Liu et al. 2011). Wave-equation migration is computationally much more efficient than reverse-time migration. With increasing computer powers, reverse-time migration is becoming more and more feasible for practical applications.

Seismic reflections/scattering from fault zones are much weaker than those from the primary

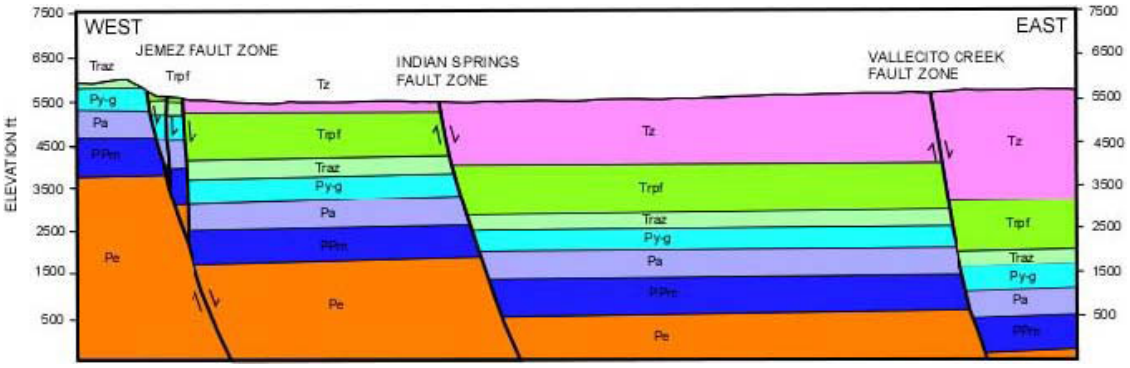

Figure 2: A geologic cross section through the Jemez fault, Indian Springs fault, and Vallecito Creek fault zones (Witcher 2004).

reflections. Therefore, it is very difficult to image steep faults. A wavefield-separation imaging condition has recently been developed for reverse-time migration using acoustic and elastic waves (Denli and Huang 2008; Liu et al. 2011). We use the reverse-time migration with a wavefield-separation imaging condition to conduct prestack migration of seismic data from Line 1 of the seismic surveys at the Pueblo of Jemez. We use the separated upgoing and downgoing waves to obtain the downward-looking images, and use the left-going and right-going waves to produce the left-looking and right-looking images, which contain significant information about fault zones. We present the preliminary results of reverse-time migration of the Line 1 data from the Pueblo of Jemez. The lateral-looking images enhance the features of the fault/fracture zones and help geologic interpretation of fault and/or fracture zones. Our results demonstrate that reverse-time migration with a wavefield-separation imaging condition can be a useful tool for exploration of geothermal resource in regions containing fault zones.

Seismic Data Acquisition

Previous geologic studies indicate that the Pueblo of Jemez contains several faults, including the Jemez fault zone, Indian Springs fault zone, and Vallecito Creek fault zone (Fig. 2). These fault zones may have controlled the flow of (hot) water of the springs in the area. The primary focus of the geothermal exploration at the Pueblo of Jemez is the area near the Indian Springs fault zone where a shallow geothermal reservoir was discovered. High-resolution imaging of these faults is essential for understanding the potential deeper geothermal system in the area. Seismic migration imaging uses seismic reflection data from active sources on the surface to produce images of subsurface geologic structures. The images show where changes in elastic properties (impedance) of geologic formations occur.

To image subsurface geologic structures of the potential target geothermal reservoir at the Pueblo of Jemez, active seismic reflection surveys were conducted in December, 2010 along three lines as depicted in Fig. 3. Lines 1 and 2 were designed to be nearly perpendicular to the Indian Springs fault zone in order to image the fault. Line 3 was along mostly the north-south direction to verify interpretations from previous geologic studies that the geologic formations in the area are dipping toward the south. Seismic data were acquired using an accelerated weight-drop seismic source (Fig. 4) and a static geophone array covering the entire lines. The spatial intervals of the sources and receivers are both 50 ft.

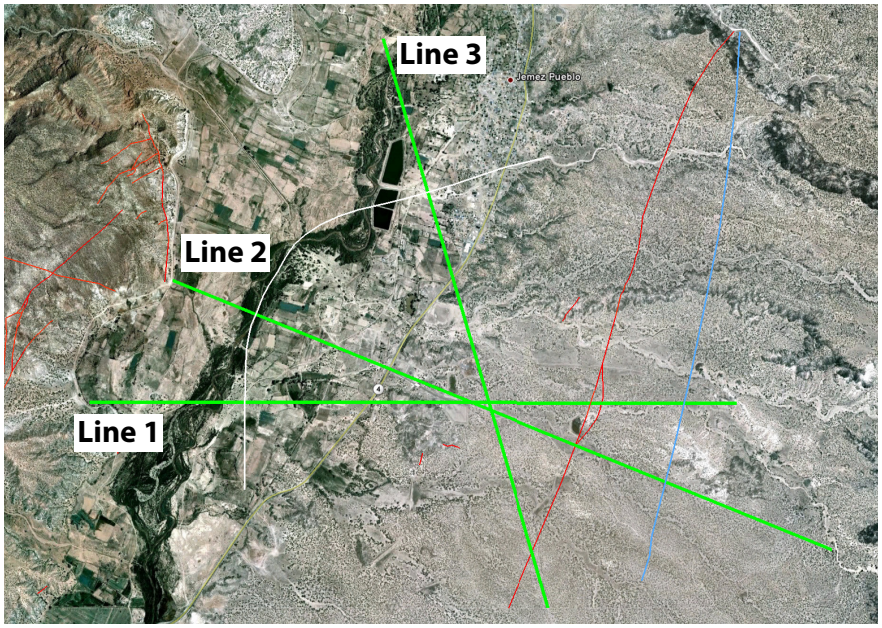

Figure 3: The three lines in green for 2D seismic reflection surveys at the Pueblo of Jemez. White curved line: Indian Springs Fault zone; Light blue line: Vallecito Creek fault zone (according to previous geologic studies); Red lines: Faults mapped during the current study.

Figure 4: An AXIS^{TM} accelerated weight-drop seismic source was used for seismic surveys.

Figure 5 shows typical seismic traces of a common-shot gather recorded along the Line 1 of the Jemez seismic surveys. Most airwaves have been removed. The white regions Fig. 5 are dead traces. Some coherent reflections in the time windows from 0.5 seconds and 1.2 seconds can be

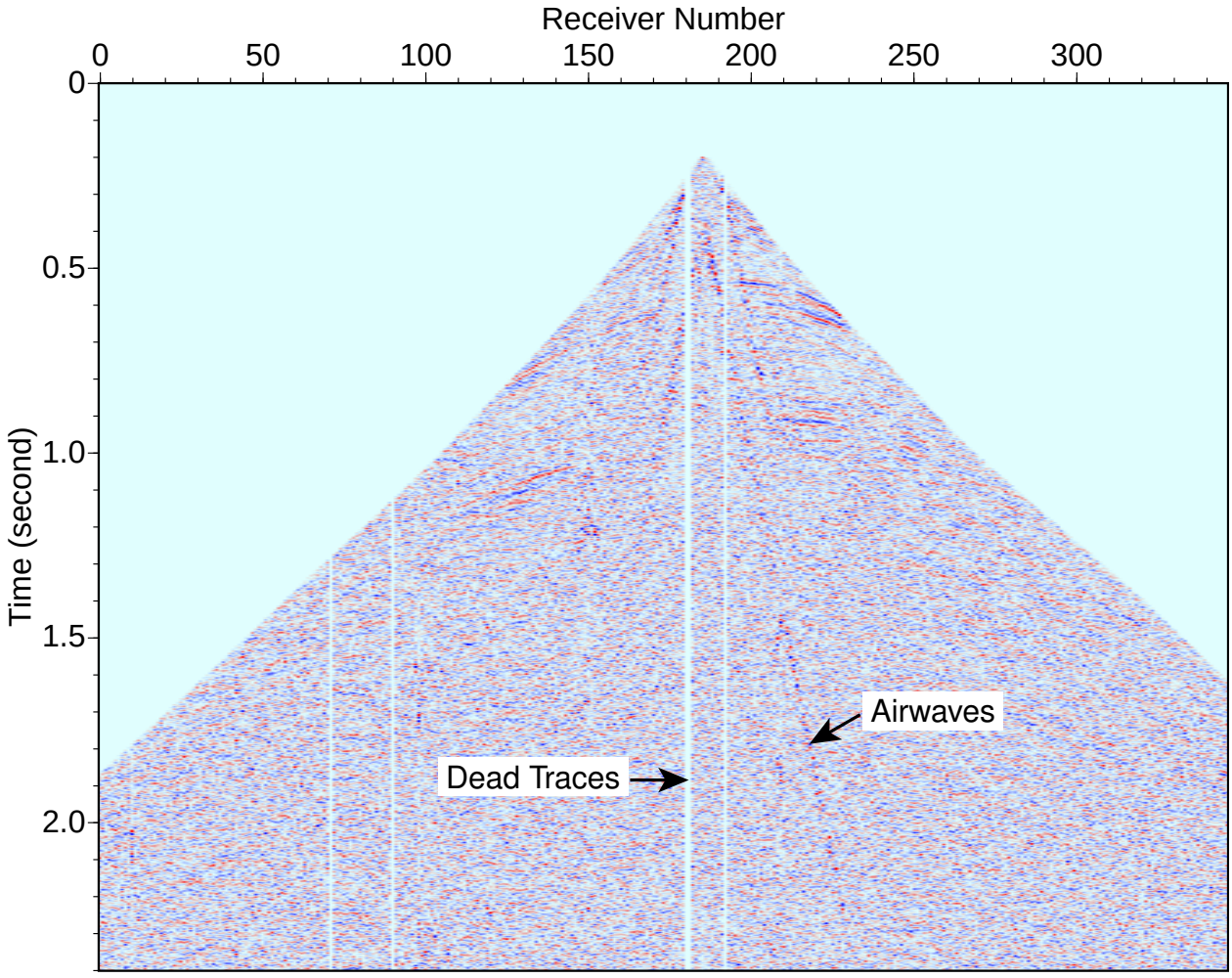

Figure 5: Typical seismic traces of a common-shot gather recorded at the Pueblo of Jemez. It contains some dead traces in the white regions, and some airwaves that cannot be removed completely.

easily identified. No significant reflections after 1.2 seconds are observed and the data contain significant noise.

Reverse-Time Migration

Forward and backward propagation of wavefields

Reverse-time migration is based on full wave equation in heterogeneous media with a constant density given by

$$\nabla^2 P(\mathbf{x},t) - \frac{1}{v^2(\mathbf{x})}\frac{\partial^2 P(\mathbf{x},t)}{\partial t^2} = f(t)\delta(\mathbf{x}-\mathbf{x}_0), \tag{1}$$

where $P(\mathbf{x},t)$ is the pressure wavefield, $\mathbf{x}$ is the spatial location, t is the time, v is the velocity, $f(t)$ is the source function or recorded data, and $\mathbf{x}_0$ is the source or receiver locations. For back-propagation of seismic data recorded at receivers on the surface of the Earth, the seismic traces are time-reversed, and the temporal sample at the maximum recording time is the first input sample.

A finite-difference scheme with a fourth-order accuracy in space and a second-order accuracy in time is used to solve equation (1). A perfectly-matching layer absorbing boundary condition is utilized to eliminate artificial reflections from the model boundaries.

Imaging condition for downward-looking images

In a target imaging region, the source and receiver wavefields obtained from forward and backward propagation using the full wave equation (1) contain waves propagating along all directions. The wavefields are decomposed into upgoing and downgoing waves:

$$\begin{aligned} S(\mathbf{x},t) &= S_d(\mathbf{x},t) + S_u(\mathbf{x},t), \\ R(\mathbf{x},t) &= R_d(\mathbf{x},t) + R_u(\mathbf{x},t), \end{aligned} \tag{2}$$

where S_d and S_u are the downgoing and upgoing waves of the forward propagating wavefields, and R_d and R_u are the downgoing and upgoing waves of the backpropagated recorded wavefields, respectively. The wavefield decomposition can be performed in the f-k_z domain where f is the frequency and k_z is the vertical component of the wavenumber along the depth direction.

The downward-looking migration image I_d is produced using

$$I_d(\mathbf{x}) = \int_0^{t_{max}} \left[S_d(\mathbf{x},t) R_u(\mathbf{x},t) + S_u(\mathbf{x},t) R_d(\mathbf{x},t) \right] dt, \tag{3}$$

where t_{max} is the maximum recording time in the data. Imaging condition (3) eliminates image artifacts of reverse-time migration with a conventional imaging condition without wavefield decomposition (Denli and Huang 2008; Liu et al. 2011).

Imaging conditions for left-looking and right-looking images

The wavefields S and R can also be decomposed into into left-going and right-going waves:

$$\begin{aligned} S(\mathbf{x},t) &= S_l(\mathbf{x},t) + S_r(\mathbf{x},t), \\ R(\mathbf{x},t) &= R_l(\mathbf{x},t) + R_r(\mathbf{x},t), \end{aligned} \tag{4}$$

where the subscripts l and r represent the left going and right going, respectively. The wavefield decomposition can be performed in the f-k_x domain where k_x is the horizontal component of the wavenumber.

Analogous to imaging condition (3), the left-looking migration image I_l is obtained by

$$I_l(\mathbf{x}) = \int_0^{t_{max}} S_l(\mathbf{x},t) R_r(\mathbf{x},t) dt, \tag{5}$$

and the right-looking migration image I_r is generated using

$$I_r(\mathbf{x}) = \int_0^{t_{max}} S_r(\mathbf{x},t) R_l(\mathbf{x},t) dt. \tag{6}$$

The left-going and right-going images contains most information of steep interfaces, such as fault/fracture zones.

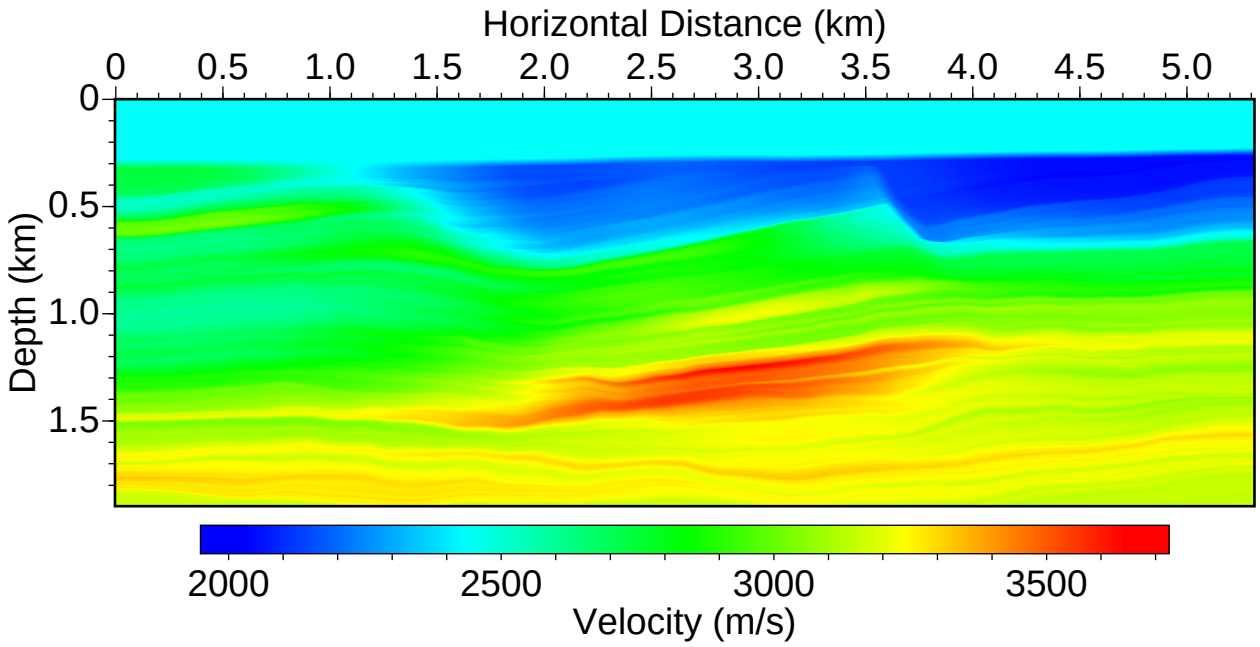

Figure 6: Velocity model

Reverse-time migration of Line 1 of Jemez seismic data

We conduct reverse-time migration of the data acquired along Line 1 (Fig. 3) of seismic surveys at the Pueblo of Jemez. The data were acquired using 317 shot points and a static seismic array with 347 receivers. Figure 6 is a velocity model obtained from migration velocity analysis of the Line 1 seismic data.

Figure 7 is a downward-looking image obtained using the upgoing and downgoing wavefields. The left-looking and right-looking images are shown in Figs. 8 and 9, respectively. Figures 8 and 9 display some image features that are not observed in Fig. 7. They enhance the images of steep interfaces, and may reveal some fault and fracture zones that cannot be seen from Fig. 7.

The geologic interpretation of migration images in Figs. 7 to 9 is depicted in Fig. 10 superimposed onto the downward-looking migration image (Fig. 7). The green lines are from the downward-looking image, the cyan lines are features enhanced by the right-looking image, and the black lines are those revealed by the left-looking image. Some of these features are in the vicinity of the faults, and could be fracture zones.

Figure 11 shows the superposition of the results of geologic mappings and Kirchhoff migration with those from reverse-time migration images (Figs. 7–9). The dipping angles of the Indian Springs fault zones from the reverse-time migration images are steeper than those from the other studies, and the positions of some of the faults move from those interpreted using a Kirchhoff migration image. In addition, our reverse-time migration uncovers a couple of faults that were overlooked before.

Conclusions

We have conducted reverse-time migration of seismic data acquired along Line 1 of surface seismic reflection surveys at the Pueblo of Jemez. A velocity model obtained from migration velocity analysis is used for migration imaging. The seismic surveys are for the exploration of a

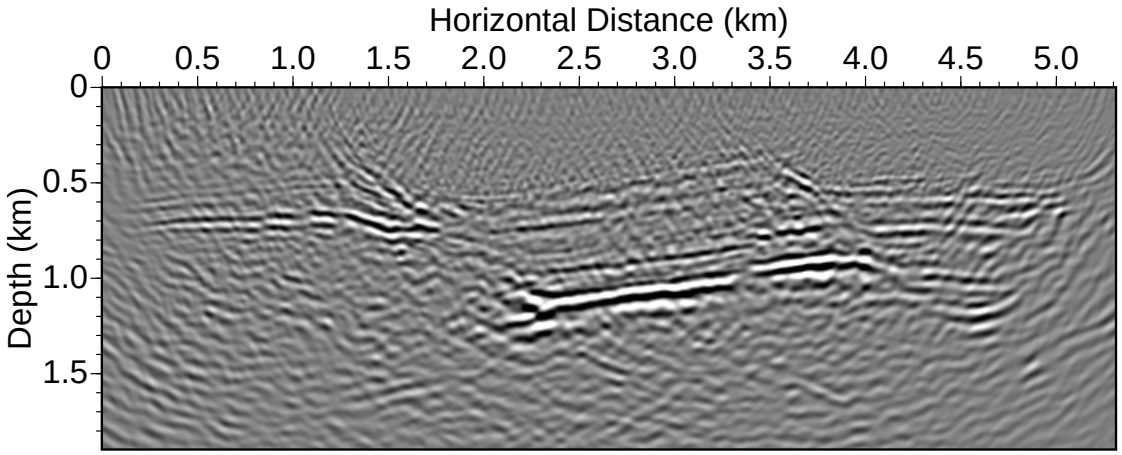

Figure 7: Downward-looking image obtained using reverse-time migration of seismic data along Line 1 of seismic surveys at Jemez Pueblo.

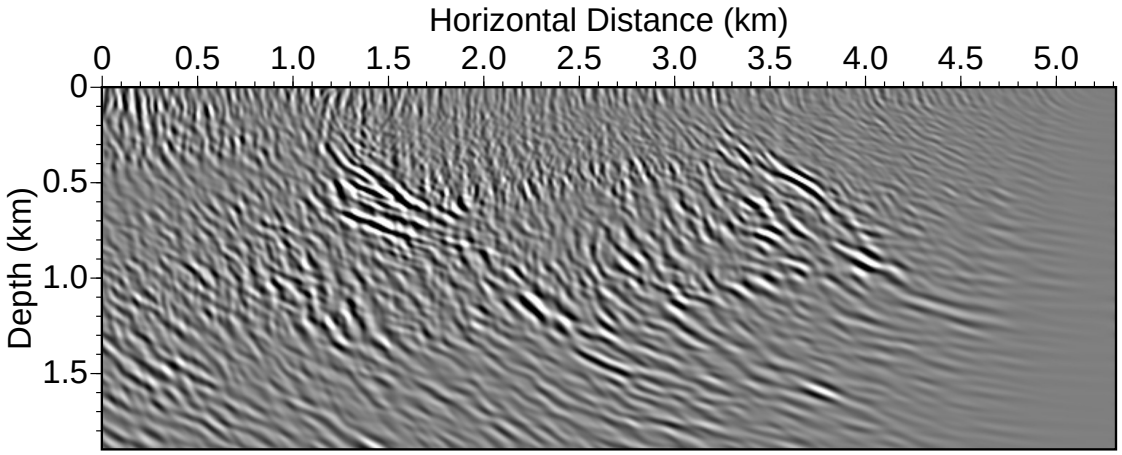

Figure 8: Left-looking image obtained using reverse-time migration of seismic data along Line 1 of seismic surveys at Jemez Pueblo.

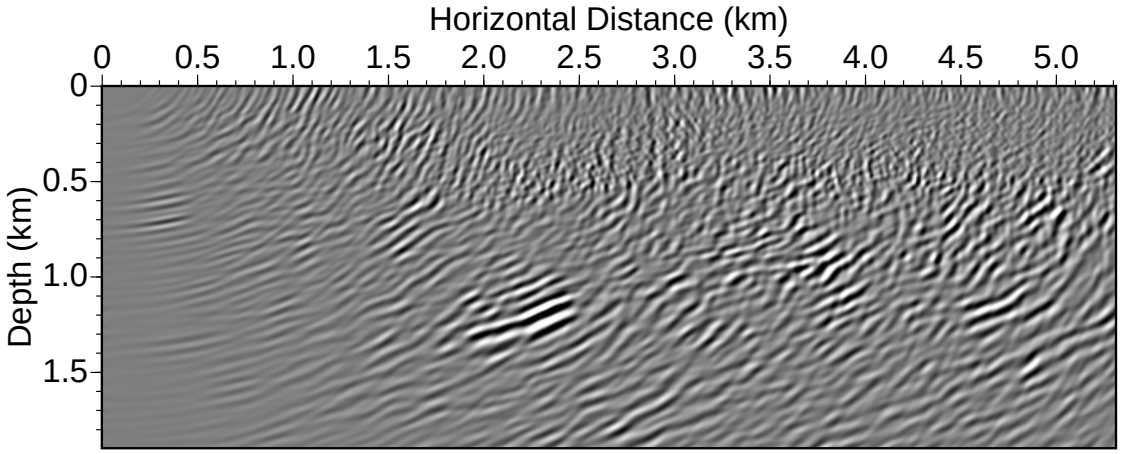

Figure 9: Right-looking image obtained using reverse-time migration of seismic data along Line 1 of seismic surveys at Jemez Pueblo.

possible deep geothermal reservoir at the Pueblo of Jemez and the primary focus is on imaging the faults zones in the area. The geologic interpretation of downward-, left-, and right-looking images obtained from reverse-time migration shows that the dipping angles of the Indian Springs fault zones are steeper than the results of the other studies. Our reverse-time migration may have revealed some fracture zones near the fault zones. In addition, our left-going and right-going migration images uncover some fault zones that were not clear before. We demonstrate that the combination of high-resolution wave-equation migration and full waveform inversion can be a powerful tool for geothermal exploration, particularly in areas with complex subsurface structures and fault zones.

The flat-datum transforms of the Jemez seismic data can introduce some errors in migration imaging. The accuracy of the velocity model obtained from migration velocity analysis can be further improved using full-waveform inversion. The reverse-time migration of the Jemez seismic data can be enhanced using a more accurate velocity model.

Acknowledgments

This work was supported by the Geothermal Technologies Program of the U.S. Department of Energy. We thank the Pueblo of Jemez for their support. We acknowledge Zonge Geosciences for seismic data acquisition and pre-processing.

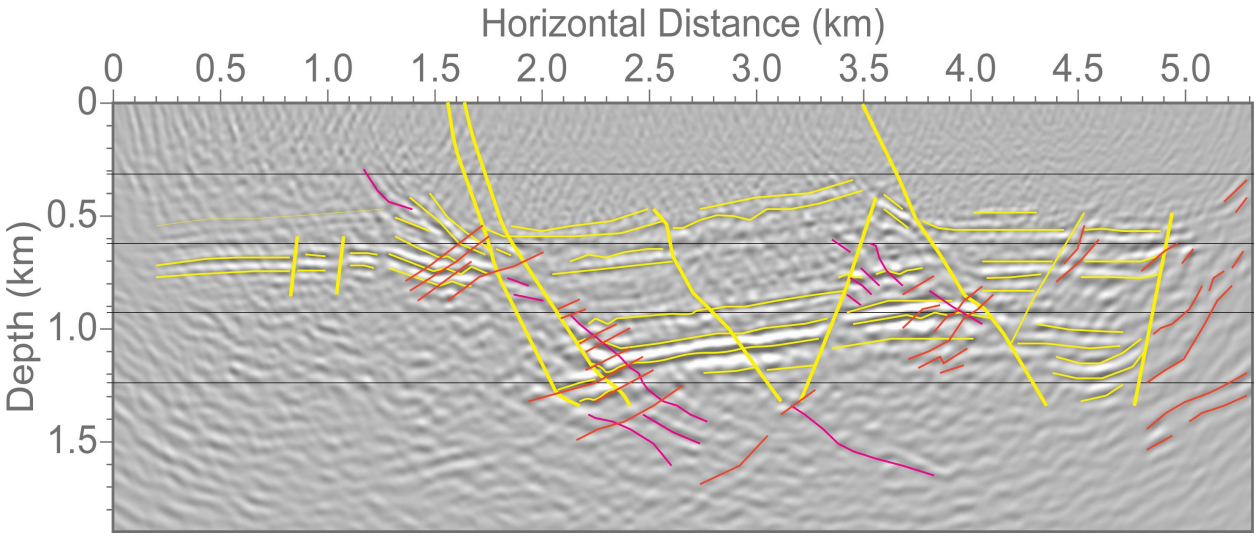

Figure 10: The faults revealed by the downward-, left- and right-looking images of reverse-time migration are superimposed onto the downward-looking image. The heavy yellow lines are faults, the light yellow lines are prominent reflectors (e.g., Pennsylvanian Madera Limestone, Permian and Triassic sandstones), the red lines are reflectors highlighted by the right-looking migration imaging, and the orange lines are the reflectors highlighted by the left-looking imaging.

References

Brown, D. W., 1993, Recent flow testing of the hdr reservoir at fenton hill, new mexico: Bulletin. Geothermal Resources Council, **22**, 208–214.

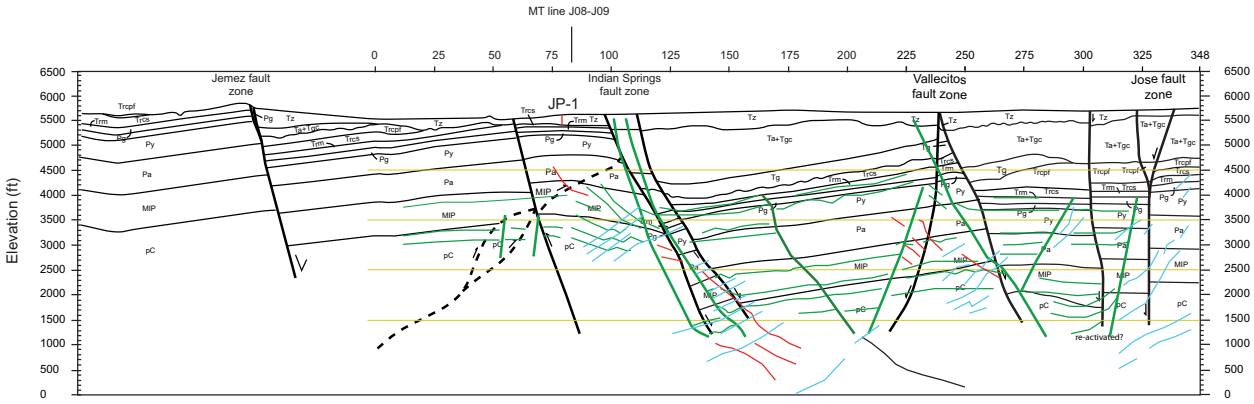

Figure 11: The faults in black are from other studies and those in color are detected using reverse-time migration.

Chang, W.-F., and G. A. McMechan, 1986, Reverse-time migration of offset vertical seismic profiling data using the excitation-time imaging condition: Geophysics, **51**, 67–84.

———, 1987, Elastic reverse-time migration: Geophysics, **52**, 1365–1375.

———, 1990, 3D acoustic prestack reverse-time migration: Geophys. Prosp., **38**, 737–755.

Claerbout, J. F., 1985, Imaging the Earth's Interior: Blackwell Scientific Publications.

Denli, H., and L. Huang, 2008, Elastic-wave reverse-time migration with a wavefield-separation imaging condition: Expanded Abstracts, 78th Annual International SEG Meeting, 30–34.

Fehler, M., and L. Huang, 2002, Modern imaging using seismic reflection data: Ann. Rev. Earth. Planet. Sci., **30**, 259–284.

Goff, F., C. Grigsby, P. J. Trujillo, D. Counce, and A. Kron, 1981, Geology, water geochemistry and geothermal potential of the jemez springs area, canon de san diego, new mexico: J. Volcanol. Geotherm. Res., **10**, 227–244.

Goff, F., and C. O. Grigsby, 1982, Valles caldera geothermal systems, new mexico, usa: J. Hydrol., **56**, 119–136.

Goff, F., L. Shevenell, J. Gardner, F. Vuataz, and C. Grigsby, 1988, Hydrothermal outflow plume of valles caldera, new mexico, and a comparison with other outflow plumes: J. Geophys. Res., **93**, 6041–6058.

Huang, L., and M. C. Fehler, 2000a, Globally optimized Fourier finite-difference migration method: 70th Ann. Internat. Mtg., Expanded Abstracts, 70th Ann. Internat. Mtg., Soc. Expl. Geophys., 802–805.

———, 2000b, Quasi-Born Fourier migration: Geophys. J. Intern., **140**, 521–534.

Huang, L., M. C. Fehler, P. M. Roberts, and C. C. Burch, 1999a, Extended local Rytov Fourier migration method: Geophysics, **64**, 1535–1545.

Huang, L., M. C. Fehler, and R. Wu, 1999b, Extended local Born Fourier migration method: Geophysics, **64**, 1524–1534.

Kerr, R. A., 1987, Hot Dry Rock: Problems, Promise: Science, **238**, 1226–1228.

Liu, F., G. Zhang, S. Morton, and J. Leveille, 2011, An effective imaging condition for reverse-time migration using wavefield decomposition: Geophysics, **76**, S29–S39.

Stoffa, P. L., J. T. Fokkema, R. M. de Luna Freire, and W. P. Kessinger, 1990, Split-step Fourier migration: Geophysics, **55**, 410–421.

Sun, H., L. Huang, and M. Fehler, 2005, Globally optimized Fourier finite-difference migration in the offset domain: Expanded Abstracts, 75th Ann. Internat. Mtg., Soc. Expl. Geophys., 1858–1861.

Sun, R., and G. A. McMechan, 2001, Scalar reverse-time depth migration of prestack elastic seismic data: Geophysics, **66**, 1519–1527.

Symes, W. W., 2007, Reverse time migration with optimal checkpointing: Geophysics, **72**, SM213–221.

Witcher, J., 2004, Pueblo of Jemez Geothermal Feasibility Project: Final Report.

Witcher, J., M. Turietta, and C. Fischer, 1992, Geothermal resources at the Pueblo of Jemez, Phase II: Reservoir assessment and feasibility of geothermal applications: Final Report prepared for CERT, Denver, CO.

Zhu, J. M., and L. R. Lines, 1997, Implicit interpolation in reverse-time migration: Geophysics, **62**, 906–917.